JACS
JOURNAL OF THE AMERICAN CHEMICAL SOCIETY
Article
pubs.acs.org/JACS

Direct and Real-Time Observation of Rotary Movement of a DNA Nanomechanical Device

Arivazhagan Rajendran,[†] Masayuki Endo,*[,‡,§] Kumi Hidaka,[†] and Hiroshi Sugiyama*[,†,‡,§]

[†]Department of Chemistry, Graduate School of Science, Kyoto University, Kitashirakawa-oiwakecho, Sakyo-ku, Kyoto 606-8502, Japan

[‡]Institute for Integrated Cell-Material Sciences (iCeMS), Kyoto University, Yoshida-ushinomiyacho, Sakyo-ku, Kyoto 606-8501, Japan

[§]CREST, Japan Science and Technology Corporation (JST), Sanbancho, Chiyoda-ku, Tokyo 102-0075, Japan

Supporting Information

ABSTRACT: Analogous to the biologically abundant protein-based linear molecular machines that translocate along their target surface, we have recently constructed the DNA-based synthetic molecular motors that effect linear movement or navigate a network of tracks on a DNA origami substrate. However, a DNA-based molecular machine with rotary function, analogous to rotary proteins, is still unexplored. Here, we report the construction of a rotary motor based on the B−Z conformational transition of DNA and the direct and real-time observation of its function within a frame-shaped DNA origami. The motor can be switched off by introducing conditions that stabilize B-DNA, while it can be fueled by adding Z-DNA-promoting high-saline buffer. When $MgCl_2$ was used as external stimulus, 70% of the motors rotated, while 76% of the stators/controls exhibited no rotation. Such a motor system could be successfully applied to perform multiple actions aimed for our benefit. Moreover, for the first time we have directly observed the B−Z conformational transition of DNA in real-time, which shed light on the fundamental understanding of DNA conformations.

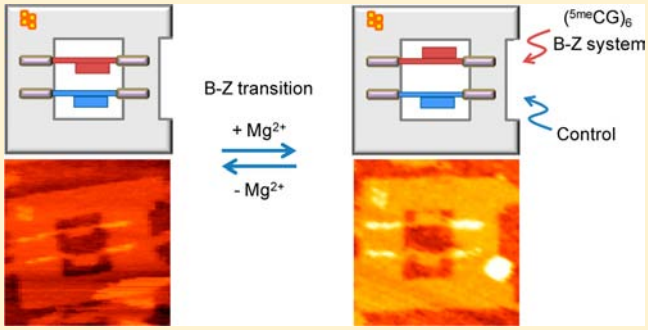

INTRODUCTION

The assembly of controllable molecular motors[1,2] with all components made of DNA is one of the central goals of structural DNA nanotechnology. The construction of linear molecular motors,[3−5] programmable DNA nanoscale assembly lines for the transport of nanoparticle cargos,[6] and molecular robots[7] was successfully demonstrated. All of these DNA motors were designed to function linearly with or without the control over the direction of progression. Nevertheless, the assembly of a rotary DNA motor/device that exhibits a controllable rotational motion has never been addressed fully. A pioneering study to achieve this goal was made by Seeman and colleagues[8] by constructing a double-crossover, antiparallel, odd-number (DAO) molecular device with B−Z transforming DNA sequence at the middle. The rotational motion of the device was characterized by monitoring the fluorescence resonance energy transfer (FRET) between the incorporated dyes. Another rotatable device, a sequence-programmable PX-JX_2 that can adopt 180° rotation, was also demonstrated by Seeman and colleagues.[6,9] However, a detailed demonstration of their rotary function, direct visualization of the entire device, and real-time analysis were unexplored. This was partly because of the technical difficulties in building such a motor and the unavailability of an appropriate characterization method, i.e., the poor spatial resolution of optical microscopy and the slow innate scan speed of conventional atomic force microscopy (AFM) were not suitable for such observations. These drawbacks are overcome in this report by the combined use of scaffolded DNA origami[10−13] and state-of-the-art high-speed atomic force microscopy (HS-AFM or Bio-AFM).[14−16] We have constructed a rotary motor based on the B−Z conformational transition of DNA. When $MgCl_2$ was used as external control, 70% of the motors rotated, whereas 76% of the stators/controls exhibited no such motion. In addition to the technical developments on the DNA rotary motor, for the first time we have directly observed the B−Z conformational transition of DNA in real-time.

EXPERIMENTAL SECTION

Chemicals and Reagents. Tris-HCl, EDTA, and $MgCl_2$ were purchased from Nacalai Tesque, Inc. (Kyoto, Japan). Single-stranded M13mp18 DNA was obtained from New England Biolabs, Inc. (Ipswich, MA, catalog no. N4040S). The staple strands (most of them are 32-mer) for the fabrication of the DNA origami frame and the oligomers for the rotor and stator preparation were received from Sigma Genosys (Hokkaido, Japan). The gel-filtration column and the sephacryl S-300 were purchased from Bio-Rad Laboratories, Inc.

Received: October 23, 2012
Published: December 19, 2012

   dx.doi.org/10.1021/ja310454k | J. Am. Chem. Soc. 2013, 135, 1117−1123

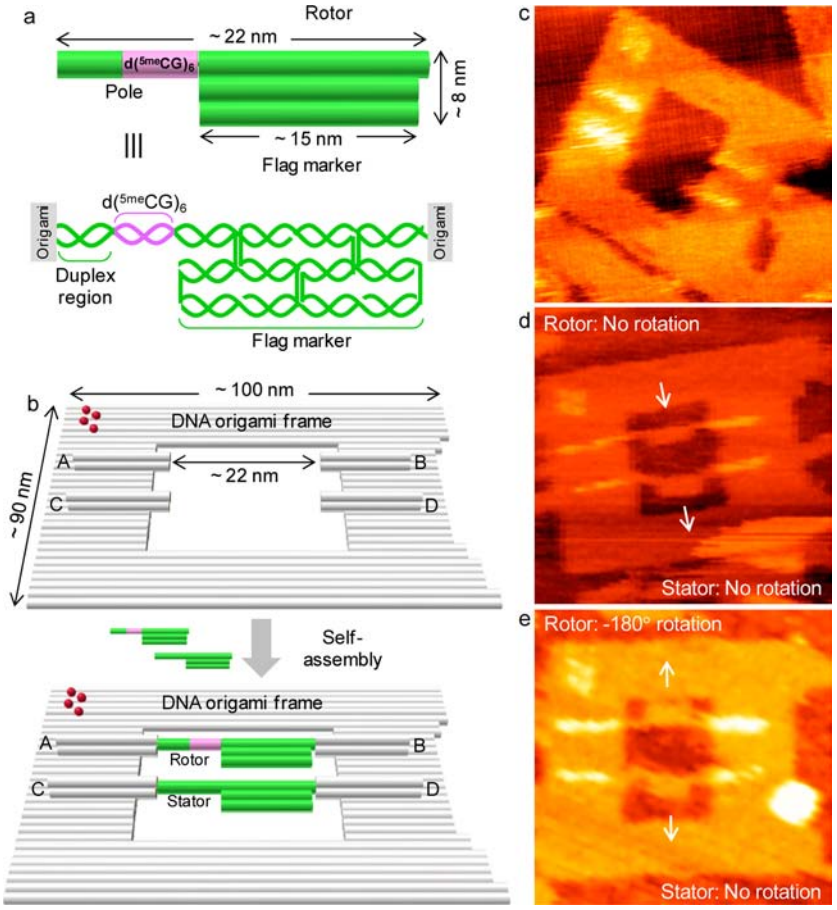

Figure 1. Schematics of the rotor and DNA origami frame and the HS-AFM images of the frame with and without the functional units. (a) Graphical explanation of the components of the rotor. The functional site in the pole region contains a $d(^{5me}CG)_6$ in the rotor. The sequences used to construct the stator were the same as that of the rotor, except that $d(^{5me}CG)_6$ was replaced with a random sequence. (b) Drawing of the DNA origami and self-assembly of the rotor and stator inside the frame. A–D are four loops in the origami frame that form two duplexes each, containing double-crossovers formed by the portion of the viral DNA with their complementary staple strands. Magenta spheres represent a set of four hairpin indexes. (c) HS-AFM image of the DNA origami frame alone. (d) Image taken after the incorporation of the rotor and stator in which both the flags face downward with respect to the pole region. (e) An image taken under the same conditions in which the stator flag faces downward, while the rotor flag faces upward. White arrows indicate the orientation of the flags. Samples were prepared in 20 mM Tris-HCl buffer (pH 7.6) containing 10 mM Mg^{2+}, and the images were recorded in the same buffer. Scan speed: 0.2 frame/s; image size: 130 × 130 nm.

(Hercules, CA) and GE Healthcare U.K. Ltd. (Buckinghamshire, U.K.), respectively. Water was deionized (≥18.0 MΩ cm specific resistance at 25 °C) by a Milli-Q system (Millipore Corp., Bedford, MA). The sequence of the hairpin index used was 5′-TCCTCTTTTGAGGAACAAGTTTTCTTGT-3′.

Preparation of the Origami Frame and Incorporation of the Rotor and Stator. Origami frame was prepared by annealing the solution of M13mp18 DNA (final concentration of 0.01 μM), staple DNA strands (4 equiv, 0.04 μM), Tris-HCl (20 mM, pH 7.6), EDTA (1 mM), and $MgCl_2$ (5–25 mM) from 85 to 15 °C at a rate of −1.0 °C/min. It was then purified using sephacryl S-300 gel-filtration column. The rotor and the stator (final concentration of 0.1 μM each) were also prepared using the same method that we have used for the preparation of the origami frame. A 10-fold excess of each rotor and stator was mixed with the purified frames. The self-assembly of these functional units inside the origami frame was carried out by annealing the solution from 45 to 15 °C at a rate of −1.0 °C/min. The flag incorporated origami was purified using sephacryl S-500 gel-filtration column before HS-AFM imaging. Gel-filtration columns were prepared in the same amount of buffer and salt with that of the origami solution that has to be purified.

AFM Imaging. AFM images were obtained using a fast-scanning AFM system (Nano Live Vision, RIBM Co. Ltd., Tsukuba, Japan) with a silicon nitride cantilever (resonant frequency 1.0–2.0 MHz, spring constant 0.1–0.3 N/m, EBD tip radius <15 nm, Olympus BL-AC10EGS-A2). The sample (2 μL) was adsorbed onto a freshly cleaved mica plate (ϕ 1.5 mm, RIBM Co. Ltd., Tsukuba, Japan) for 5 min at room temperature and then washed several times using the same buffer solution with same concentration of $MgCl_2$ with that of the origami was prepared. Scanning was performed using the tapping mode in the same buffer solution.

CD Spectra. The CD spectra of the $d(^{5me}CG)_6$ (2 μM of dsDNA) in Tris-HCl buffer (20 mM, pH 7.6) containing $MgCl_2$ (0–50 mM) were obtained using a J-805LST spectropolarimeter (JASCO Co., Ltd., Japan) with 1 cm path length quartz cell at 5 °C. The cuvette-holding chamber was flushed with a constant stream of dry N_2 gas to avoid water condensation on the cuvette surface. Data were collected from 200 to 400 nm with 4 s response time, 1 nm slit width, and a scan speed of 100 nm/min. Each spectrum shown is the average of three individual scans and is buffer corrected.

RESULTS AND DISCUSSION

The Design of Rotor, Stator, and DNA Origami Frame. The nanostructures prepared by the scaffolded DNA origami method served as novel substrates for various biomolecular analyses at single-molecular level[5,17−19] and for the nanopatterning of functional molecules and nanoparticles.[20] They have also shown to be useful substrates for the construction of

dx.doi.org/10.1021/ja310454k | J. Am. Chem. Soc. 2013, 135, 1117−1123

automated molecular motors.[3,4,6,7] Due to the structural flexibility and stability in various environments,[11,21,22] we have adopted the DNA origami structures for our nanodevice construction.

We have constructed a flag-shaped DNA rotary nanomechanical device that is incorporated within a frame-shaped DNA origami[17−19] and directly visualized its function in real-time. The outlines of the functional motor and origami frame are given in Figure 1a,b (for detailed design see Figures S1−S2). The device consists of a B-DNA region forming the bottom part of the pole of the flag, a B−Z transforming functional site that shares the pole region and is responsible for the rotational motion, analogous to the gear of an automobile, a flag-shaped marker composed of three duplexes that are connected through crossovers, and single-stranded overhangs at both the termini that can assist the catenation of the whole motor assembly inside the DNA origami frame. For the construction of the B−Z region, we used the base-paired sequence $d(^{5me}CG)_6$ in which the cytosines are methylated at the 5-position. This modification was shown to enhance the formation of Z-DNA at lower salt environments, because the methyl group strengthen hydrophobic interactions.[23,24] Further, in a Z-form DNA, the bases alternate in *syn* and *anti* conformations while all the bases adopt the *anti* conformation in a B-DNA.[25−30] *Syn* conformation is more stable for purines than that of pyrimidines, and thus, alternating purine and pyrimidine bases readily adopt Z conformation.[31] Therefore in the present study, we have adopted the alternating ^{5me}C and G bases. The flag marker was introduced at a position where it can be visible in the AFM topographical image in conditions in which the motor is switched off. When the motor is in action, the flag marker rotates around the pole, and the rotary motion can be tracked by monitoring the orientation of the flag. The length of the device is about 22 nm, and the size of the flag is about 15 nm in length and 8 nm in width. In addition to the rotary motor, a nonfunctional stator/control, which is similar to the motor except that it has a random sequence instead of the B−Z functional site, was also prepared.

Regarding the origami design, we have adopted Rothemund-type DNA origami,[10,11,32] which consists of 30 duplexes with a central cavity, forming a frame structure (Figure 1b). In order to connect the functional rotary device and its counterpart nonfunctional stator, we introduced four loops in the origami frame (namely A−D) that form two duplexes each, containing double-crossovers formed by the portion of M13 viral DNA with their complementary staple strands.[32] These loops were placed vertically on the origami frame surface, so that the rotor and stator can be anchored far from the mica surface. This spatial arrangement was imposed in the origami design, so as to reduce the interactions of the motor components with the mica surface and to provide sufficient space for the motor to rotate freely. Further, the origami was designed in such a way that simultaneous analysis of the rotor and stator can be performed, ignoring the possibility of uncertainty in the analysis. To match the length of the motor, the distance between two loops (for example, A and B) was designed to be 64 base pairs. To distinguish the motor and stator, the origami was indexed with a set of four hairpin DNAs at the top left corner.

Preparation of the Motor Assembly. The origami frame was fabricated by folding the M13mp18 viral genome using about 200 staple strands.[11] The motor and stator were also prefolded under similar conditions. After removing the excess staples from the origami solution, a 10-fold excess of each motor and stator were mixed with the origami. The second annealing yielded the final rotor and stator assemblies inside the origami frame. The HS-AFM analyses were performed after removing the excess amount of unbound rotor and stator in solution (for further details, see Experimental section).

Static Analysis of Rotary Function. At first, we have characterized the formation of origami frame, and the incorporation of the motor and stator inside the frame at 10 mM Mg^{2+}. We used Mg^{2+} ions due to the fact that they can facilitate the binding of origami on mica surface and also they bind to the CG repeat sequence through a hydration shell with up to three hydrogen bonds to guanine N7 and O6 to stabilize the Z-DNA.[33] The origami frame was formed as designed (Figure 1c), and the incorporation of the flags was successful (Figure 1d). The flag shape of the motor and stator can be readily seen in the HS-AFM image, and the measured dimensions of the flags were in good agreement with the original design. Notably, both the motor and stator flags adopted the downward orientation with respect to the hairpin index/pole region (Figure 1d). In several instances, the motor flags were seen to adopt the upward orientation as well (Figure 1e), which is due to −180° rotation around the pole. In contrast, the stator flags adopted the downward orientation in most cases. In order to obtain the statistically meaningful values, we counted both the flags based on their relative orientations in 10 mM Mg^{2+}. We found that majority of the motors (60%) adopted upward orientation, while in contrast, 70% of the stators adopted downward orientation (Figure 2, and Figure S3). This indicated that at this salt concentration, the motor was already in action and adopted rotational motion, whereas the stator had no such movement; however, some stators may display Brownian-like motion.

Salt-Dependent Studies. To verify this, the experiments were carried out with lower (where B-DNA is predominant) and higher (where Z-DNA is stabilized) salt concentrations. At 5 mM Mg^{2+}, an abrupt change in the ratio between the upward and downward orientations of the motor flags was observed, where only 29% of the flags adopted the upward orientation. However, an increasing amount of upward orientation was observed for the motor when the salt concentration was increased from 10 to 25 mM. Irrespective of the salt concentration, 70−76% of the stator flags adopted the downward orientation (Figures 2 and S3). This observation clearly indicated the dynamic nature of the motor, while the stator was almost static. As shown in Figure 2a, the stator defines the lower (about 25%) and higher (about 75%) boundaries, and the rotor exhibits its function within those boundaries. Note that the yield calculations of the flag orientations were performed using the images that were recorded at different time scales. Because of its dynamic nature, the flag orientation may be changed at different times, and thus, there may be an uncertainty in the calculated values. However, the flags have equal probability for the forward and backward movements, i.e., when a flag moves upward, another flag has equal chance to rotate downward. Thus, it may avoid the errors in the calculated yields. Further, we have adopted similar methods to calculate the yields at different salt concentrations, thus nullifying the uncertainties.

Circular Dichroic Spectral Studies. To confirm that the amount of salt we used is sufficient to initiate B−Z transition, we recorded the circular dichroic spectra of a similar sequence $d(^{5me}CG)_6$ that had no flanking base at either terminus. The transition midpoint was obtained at ∼4 mM of Mg^{2+} (Figure

dx.doi.org/10.1021/ja310454k | J. Am. Chem. Soc. 2013, 135, 1117−1123

a

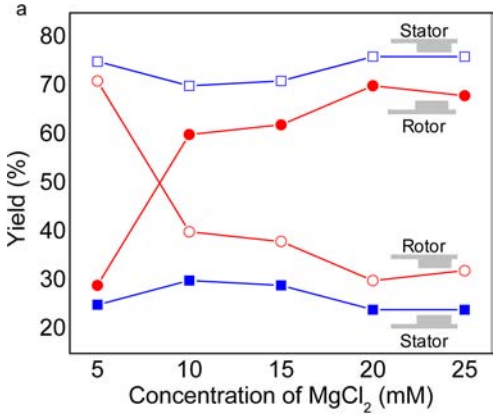

b

Concentration of Mg^{2+} (mM)	Rotor (%)		Stator (%)	
5	71	29	75	25
	Flags counted: 70		Flags counted: 68	
10	40	60	70	30
	Flags counted: 163		Flags counted: 171	
15	38	62	71	29
	Flags counted: 84		Flags counted: 86	
20	30	70	76	24
	Flags counted: 121		Flags counted: 116	
25	32	68	76	24
	Flags counted: 62		Flags counted: 63	

Figure 2. Salt-dependent changes in the flag orientations. (a) The plot of the orientations of rotor and stator flags at different concentrations of $MgCl_2$ as estimated from the HS-AFM images. Stator flag orientation is independent of the salt concentration with ~75% of the flags adopting the downward orientation, while about 25% are in the upward orientation. The rotor flag is highly dynamic and adopts upward orientation upon increasing the salt concentration. (b) The yields of the flag orientations are tabulated. For representative AFM images, see Figure S3.

S4), which is lower than the concentrations we used for AFM imaging. Further, the transition was fully completed with 12.5 mM of Mg^{2+}. It is obvious to expect that the motor may require a higher amount of salt because the B−Z functional site is flanked by several bases at both ends. However, the ensemble analysis adopts the DNA concentration in the order of micromolar that may require a higher salt concentration to neutralize the negative charges of phosphate backbone.[24] In contrast, in our single-molecule analysis, the concentration of the motor assembly on mica surface is expected to be in the order of picomolar which may require relatively lower amount of salt. Thus, it is not appropriate to compare the bulk and single-molecule environments, while it is apparent to consider the charge ratio between the DNA and the salt rather than the overall concentration. Hence, we believe that the salt concentrations we used are sufficient to fuel the rotary motor as evidenced by HS-AFM imaging. Indeed, it seems that the B−Z transition midpoint of our motor functional unit lies around the concentration of 8 mM Mg^{2+}, and the transition may be completed at the saturating salt concentration of 20 mM Mg^{2+} (Figure 2).

Real-Time Analysis of the Dynamics of Rotary Motor. After characterizing the rotary motion using the static images, we conducted dynamic imaging analysis to monitor the function of the rotor and the intermediate states involved. The real-time observation was carried out with an image acquisition frequency of 0.2 frame/s. The origami frame with incorporated motor and stator was prepared in a buffer that contained 10 mM Mg^{2+}. The assembly was then deposited onto a mica surface and imaged under a liquid condition which contained the same amount of buffer and salt with that of the origami solution. It is obvious to use such a salt concentration where the functional unit could be in equilibrium between the B- and Z-forms of DNA, which may slowdown the rotational motion and consequently make the real-time analysis relatively easy. The snapshots of the HS-AFM images recorded are shown in Figure 3a (see Supporting Information movie). The dynamic nature of the rotor can be clearly seen from the images. At 0 s, both the motor and stator flags adopted the downward orientation, assigned to be the initial B-conformation. The downward orientation of the rotor flag was maintained until 20 s, where no dynamics was observed. The rotation was started at 25 s, where the flag shape of the rotor seems to disappear partly and was clearly seen to adopt the upward orientation at 30 s. This upward orientation of the rotor corresponds to a rotation of about −180°, making a half turn. The same orientation was retained for few seconds and the rotation was continued to yield the downward orientation at 40 s. At this point, the rotor either reversed its position back to the initial state by rotating 180° or continued a further rotation of −180° to complete a full turn. It should be noted that the shape of the rotor flag was not so clear, and it was difficult to estimate its orientation at 25 and 35 s. This could possibly be due to the dynamic nature of the flag and may correspond to partly rotated states between downward and upward orientations. The downward orientation was retained until 75 s, and the flag seems to adopt the intermediate rotation at 80 s where its position is again unambiguous. At 85 s, the flag was found to be in the upward position, which may correspond to either a half turn (if it was reverted its position in the first instance of rotation) or −1.5 turn (if it completed a full turn of rotation in the first instance) of the rotor. The final rotation was observed at 120 s, where the rotor flag adopted the downward orientation again, completing two full cycles of rotation or just adopting half turn and then reverting it back. Interestingly, the stator flag adopted exclusively downward orientation throughout the imaging, indicated that it has no rotary motion because no conformational change can be possible, and thus, validating the rotary function of the motor system. The clear appearance of the stator flag over motor flag in the AFM images further indicated the static behavior of the stator.

Distance and Height Profiles. The dynamic nature of the rotor and the static behavior of the stator can also be seen from the distances estimated between the flags and origami frame, as illustrated in Figure 4a. The estimated lowest and highest distances for the rotor are in good agreement with the expected values of 7 and 21 nm, respectively. Also, due to the static nature, the stator is expected to have a constant distance of 10 nm, and the measured distances are in good agreement with the expected value. Further, we could often reproduce such rotations of the rotor (Figure S5). We also estimated the heights of the rotary motor and stator from the time-lapse images (Figure 4b). The stator displayed the lowest height and was nearly constant throughout the imaging, whereas the rotary motor displayed relatively higher height and often was increased up to 1 nm. Such an increase in the height could correspond to the vertical orientation (about −90°) of the flag with respect to the origami frame, indicating out-of-plane rotation of the rotor. Moreover, the height profiles estimated along the pole region of the rotor (Figure 4c) were also

dx.doi.org/10.1021/ja310454k | J. Am. Chem. Soc. 2013, 135, 1117−1123

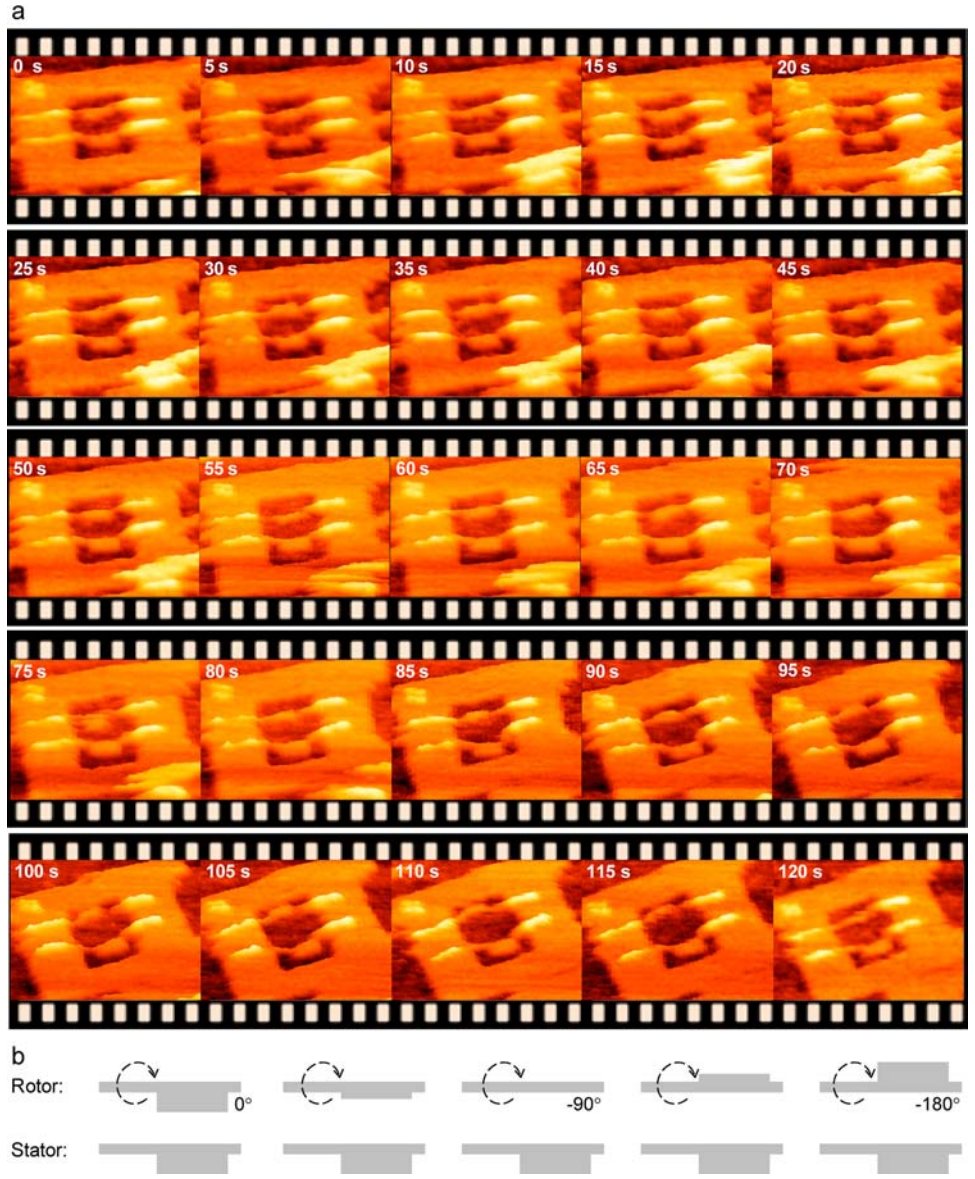

Figure 3. Snapshots of the HS-AFM imaging and schematics of the molecular events during rotary motor action. (a) Time-lapse images recorded at a scan speed of 0.2 frame/s. [Tris-HCl] = 20 mM (pH 7.6), [Mg^{2+}] = 10 mM, image size: 150 × 110 nm. (b) Graphical explanation of the molecular events during the rotor flag rotation of −180°. The rotor exhibited out-of-plane rotation, while the stator was static throughout the imaging.

supported the same conclusion. The estimated increase in height of ∼1 nm is lower than the expected value of about 6 nm. This indicates that the flag rotates faster than the scan rate of 5 s/frame. Moreover, because of its dynamic nature, it is difficult to locate the rotor flag orientation precisely when it is vertical, and the cantilever may sometimes distract the rotor flag as can be seen in Figure 3a, at 75 s.

It is worth mentioning here that the change in helical twist from B- to Z-DNA transition was estimated to be about −128° for each dinucleotide of d(CG),[34] and thus, the expected twist for the functional site with six dinucleotide repeats that we adopted could be roughly −2.1 turns (excluding the twist at the B-Z junction). By considering this fact and the real-time HS-AFM images that we recorded, we anticipate that our motor adopted two full rotations, one from 0 to 40 s and the other from 40 to 120 s. The first cycle of rotation is about twice as fast as the latter cycle. Further, the overall time required for the completion of two full rotations is about 120 s seems to be long. This could be possibly because the motor system was immobilized on mica surface, and the interaction of the motor components-surface may slowdown the rotary action. In addition, the amount of salt we used may not be sufficient to rotate the flag rapidly, and we anticipate that saturating salt concentration may speed up the motor rotation as evidenced by the preliminary analysis performed at 20 mM Mg^{2+} (Figure 2). Further, the d(^{5me}CG) repeat sequence that we used is relatively shorter, thus preventing the fast rotation of the rotor.

It has been shown that Z-DNA exists in two different forms called Z_I and Z_{II} that differ in their rotation of phosphate group in a CG repeat sequence.[35] Form Z_{II} was found to occur in the presence of Mg^{2+}, and thus we anticipate that the functional site of our rotor may adopt a Z_{II} conformation. The left-handed Z-form is one of the characteristic and significant local conformations of DNA. It has been extensively studied in relation to methylation of cytosine, transcription, and the level of DNA supercoiling. However, the precise biological function

dx.doi.org/10.1021/ja310454k | J. Am. Chem. Soc. 2013, 135, 1117−1123

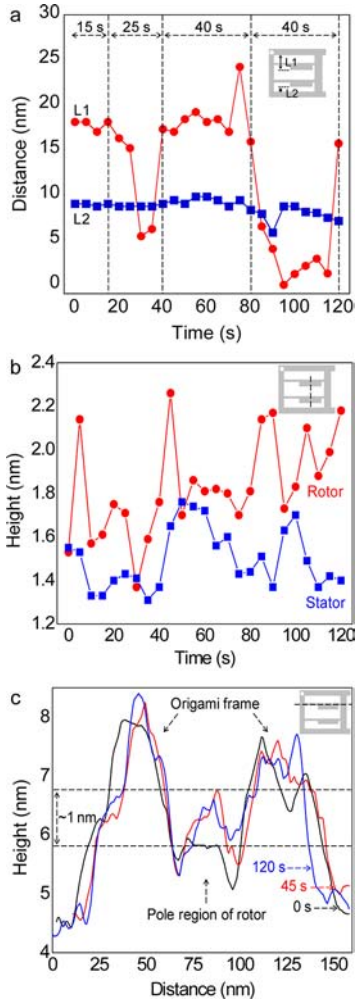

Figure 4. Trajectories of the distances and height profiles of the flags. (a) The distances between the edges of a rotor (L1) or a stator (L2) flags and the origami frame (see inset). The static behavior of the stator and the dynamic nature of the rotor can be readily seen. (b) The heights of the rotor and stator flags during successive imaging. Dotted line in the inset indicates the positions where the heights were estimated. (c) The height profile along the pole region (indicated by the dashed line in the inset) of the rotor as estimated at 0, 45, and 120 s. The time-lapse images given in Figure 3a were used for these analyses.

of the Z-DNA in living cell and the B-Z transition have not been fully understood, probably due to the lack of proper detection method. Here, for the first time we have directly observed the B−Z conformational transition of DNA in real-time. We believe that this report could improve our basic knowledge on the conformations of DNA.

Regarding the real-time analysis, there are several new findings in the real-time observation when compared to the static observation: (i) dynamics of the rotor cannot be visualized in the static observation, while it can be monitored in the real-time analysis; (ii) in static observation, it is possible to see the flag rotation of −180° only. However, we could monitor the complete function or the two full rotations (360° × 2) in case of real-time observation; (iii) in static observation, it is difficult to estimate the time required for each rotation, while it is possible in case of real-time analysis, at least a rough estimation; (iv) in real-time observation, it is possible to confirm that the rotor alone rotates, while the stator has no rotational motion. Such a relative comparison is difficult with static observation; (v) the intermediate rotations such as −90° is not possible to see in case of static observation, where as it is possible in case of real-time analysis; and (vi) monitoring the biological phenomena at real-time promises to offer several information and is one of the goals for scientists in various disciplines. Such a real-time analysis is not possible with most available techniques, and our results describe one of the few examples available. Though it is not providing all possible information, it is rather a good initiation.

CONCLUSION

In concluding remarks, we would like to highlight the pros and cons of our rotary motor. The synthetic DNA molecular motors that mimic the biologically relevant protein-based linear motors have been constructed based on the base-pairing principles of DNA, for instance, toehold-mediated branch migration.[3,4,6,7] However, the rotary motor that we have developed here relies on the genetic information that is stored in DNA in the form of conformation (for instance B−Z conformational transition). In order to function, the protein motors require the hydrolysis of ATP,[15,36,37] while the DNA motors developed thus far require enzymes to cleave the stator strands.[3,4,7] Similar to these systems, the function of our rotary motor can be controlled by the concentration of the metal cations. Rotor function can also be controlled by the external stimuli, such as Z-DNA-binding synthetic ligands,[38] the Zα domain of human ADAR1 protein, or any other protein that stabilizes the Z-form of DNA, indicating the ability of the motor to function in a biologically relevant environment. As an alternative to the modified cytosine, one can use ^{8me}G to construct the B−Z functional site.[39] To date, a detailed real-time analysis was carried out only for a protein motor, the rotorless F_1-ATPase that rotates in-plane.[37] Irrespective of the biomolecules (protein or DNA) that were used for the construction of the motors, we present here the first example in which a direct and real-time analysis was conducted on the motor function that has out-of-plane rotational motion. Although AFM is a topographical imaging technique, our results indicate that it can also be successfully applied for the analysis of out-of-plane rotations. The previous device construction and its analysis using FRET technique restricts the rotation of the device to be an odd number of half turns, so that the incorporated dyes can be placed far from each other and that the output signal can be readout.[8] However, our device construction and the HS-AFM-based analysis give us the freedom to incorporate any number of half turns due to the fact that the rotation of the motor can be traced out at any point. We have also proved that the device can be incorporated in larger nanostructures, such as DNA origami, in order to achieve complex molecular machinery. We have previously shown that the DNA origami structures can be lyophilized, stored, and reused when required.[11] Thus, it is possible to store the lyophilized sample of our rotary motor assembly inside DNA origami frame and reused when required. Though the motor function was directly monitored, the information on the direction of the motor rotation was not observed. Besides this disadvantage, we believe that the construction of the rotary motor and its real-time analysis with unprecedented spatial and temporal resolution will strengthen the concept of molecular motors based on conformational changes of DNA. We anticipate that this motor can be successfully applied to carry

out several automated functions, such as molecular transport, that rely on rotational motion.

■ ASSOCIATED CONTENT

Supporting Information

Additional information as noted in text. This material is available free of charge via the Internet at http://pubs.acs.org.

■ AUTHOR INFORMATION

Corresponding Author

endo@kuchem.kyoto-u.ac.jp; hs@kuchem.kyoto-u.ac.jp

Notes

The authors declare no competing financial interest.

■ ACKNOWLEDGMENTS

We express our sincere thanks for the CREST grant from the Japan Science and Technology Corporation (JST), grants from the WPI program (iCeMS, Kyoto University), and Grant-in-Aid for Scientific Research from the Ministry of Education, Culture, Sports, Science and Technology (MEXT), Japan. Financial support from Nagase Science and Technology Foundation to M.E. is also acknowledged. A.R. expresses sincere thanks to the Japan Society for the Promotion of Science (JSPS) for the Postdoctoral fellowship. We thank Sekar Latha for her help with the graphics.

■ REFERENCES

(1) Murakami, H.; Kawabuchi, A.; Kotoo, K.; Kunitake, M.; Nakashima, N. *J. Am. Chem. Soc.* **1997**, *119*, 7605.

(2) Bissell, R. A.; Cordova, E.; Kaifer, A. E.; Stoddart, J. F. *Nature* **1994**, *369*, 133.

(3) Wickham, S. F. J.; Endo, M.; Katsuda, Y.; Hidaka, K.; Bath, J.; Sugiyama, H.; Turberfield, A. J. *Nat. Nanotechnol.* **2011**, *6*, 166.

(4) Wickham, S. F. J.; Bath, J.; Katsuda, Y.; Endo, M.; Hidaka, K.; Sugiyama, H.; Turberfield, A. J. *Nat. Nanotechnol.* **2012**, *7*, 169.

(5) Rajendran, A.; Endo, M.; Sugiyama, H. *Angew. Chem., Int. Ed.* **2012**, *51*, 874.

(6) Gu, H.; Chao, J.; Xiao, S.-J.; Seeman, N. C. *Nature* **2010**, *465*, 202.

(7) Lund, K.; Manzo, A. J.; Dabby, N.; Michelotti, N.; Johnson-Buck, A.; Nangreave, J.; Taylor, S.; Pei, R.; Stojanovic, M. N.; Walter, N. G.; Winfree, E.; Yan, H. *Nature* **2010**, *465*, 206.

(8) Mao, C.; Sun, W.; Shen, Z.; Seeman, N. C. *Nature* **1999**, *397*, 144.

(9) Gu, H.; Chao, J.; Xiao, S.-J.; Seeman, N. C. *Nat. Nanotechnol.* **2009**, *4*, 245.

(10) Rothemund, P. W. *Nature* **2006**, *440*, 297.

(11) Rajendran, A.; Endo, M.; Sugiyama, H. *Curr. Protoc. Nucleic Acid Chem.* **2012**, *48*, 12.9.1.

(12) Rajendran, A.; Endo, M.; Hidaka, K.; Sugiyama, H. *Chem. Commun.* **2013**, *49*, 686.

(13) Endo, M.; Sugita, T.; Rajendran, A.; Katsuda, Y.; Emura, T.; Hidaka, K.; Sugiyama, H. *Chem. Commun.* **2011**, *47*, 3213.

(14) Yamamoto, D.; Uchihashi, T.; Kodera, N.; Yamashita, H.; Nishikori, S.; Ogura, T.; Shibata, M.; Ando, T. *Methods Enzymol.* **2010**, *475*, 541.

(15) *Structural and functional analysis of proteins by high-speed atomic force microscopy*; Rajendran, A., Endo, M., Sugiyama, H., Eds.; Acdademic Press, Elsevier: Waltham, MA, 2012; Vol. *87*, pp 5−55.

(16) Dhakal, S.; Mao, H.; Rajendran, A.; Endo, M.; Sugiyama, H. In *Guanine Quartets: Structure and Application*; The Royal Society of Chemistry: London, 2013; Vol. *0*, p 73.

(17) Sannohe, Y.; Endo, M.; Katsuda, Y.; Hidaka, K.; Sugiyama, H. *J. Am. Chem. Soc.* **2010**, *132*, 16311.

(18) Endo, M.; Katsuda, Y.; Hidaka, K.; Sugiyama, H. *J. Am. Chem. Soc.* **2010**, *132*, 1592.

(19) Endo, M.; Katsuda, Y.; Hidaka, K.; Sugiyama, H. *Angew. Chem., Int. Ed.* **2010**, *49*, 9412.

(20) Endo, M.; Yang, Y.; Emura, T.; Hidaka, K.; Sugiyama, H. *Chem. Commun.* **2011**, *47*, 10743.

(21) Mei, Q.; Wei, X.; Su, F.; Liu, Y.; Youngbull, C.; Johnson, R.; Lindsay, S.; Yan, H.; Meldrum, D. *Nano Lett.* **2011**, *11*, 1477.

(22) Rajendran, A.; Endo, M.; Katsuda, Y.; Hidaka, K.; Sugiyama, H. *J. Am. Chem. Soc.* **2011**, *133*, 14488.

(23) Zacharias, W.; Jaworski, A.; Wells, R. D. *J. Bacteriol.* **1990**, *172*, 3278.

(24) Behe, M.; Felsenfeld, G. *Proc. Natl. Acad. Sci.* **1981**, *78*, 1619.

(25) Rajendran, A.; Magesh, C. J.; Perumal, P. T. *Biochim. Biophys. Acta, Gen. Subj.* **2008**, *1780*, 282.

(26) Rajendar, B.; Rajendran, A.; Sato, Y.; Nishizawa, S.; Teramae, N. *Bioorg. Med. Chem.* **2009**, *17*, 351.

(27) Thiagarajan, V.; Rajendran, A.; Satake, H.; Nishizawa, S.; Teramae, N. *ChemBioChem* **2010**, *11*, 94.

(28) Rajendran, A.; Thiagarajan, V.; Rajendar, B.; Nishizawa, S.; Teramae, N. *Biochim. Biophys. Acta, Gen. Subj.* **2009**, *1790*, 95.

(29) Rajendran, A.; Zhao, C.; Rajendar, B.; Thiagarajan, V.; Sato, Y.; Nishizawa, S.; Teramae, N. *Biochim. Biophys. Acta, Gen. Subj.* **2010**, *1800*, 599.

(30) Rajendar, B.; Rajendran, A.; Ye, Z.; Kanai, E.; Sato, Y.; Nishizawa, S.; Sikorski, M.; Teramae, N. *Org. Biomol. Chem.* **2010**, *8*, 4949.

(31) Lee, M.; Kim, S. H.; Hong, S.-C. *Proc. Natl. Acad. Sci.* **2010**, *107* (11), 4985.

(32) Rajendran, A.; Endo, M.; Katsuda, Y.; Hidaka, K.; Sugiyama, H. *ACS Nano* **2011**, *5*, 665.

(33) Gessner, R. V.; Quigley, G. J.; Wang, A. H. J.; Van der Marel, G. A.; Van Boom, J. H.; Rich, A. *Biochemistry* **1985**, *24*, 237.

(34) Rich, A.; Nordheim, A.; Wang, A. H. J. *Annu. Rev. Biochem.* **1984**, *53*, 791.

(35) Wang, A.; Quigley, G.; Kolpak, F.; van der Marel, G.; van Boom, J.; Rich, A. *Science* **1981**, *211*, 171.

(36) Kodera, N.; Yamamoto, D.; Ishikawa, R.; Ando, T. *Nature* **2010**, *468*, 72.

(37) Uchihashi, T.; Iino, R.; Ando, T.; Noji, H. *Science* **2011**, *333*, 755.

(38) Xu, Y.; Zhang, Y. X.; Sugiyama, H.; Umano, T.; Osuga, H.; Tanaka, K. *J. Am. Chem. Soc.* **2004**, *126*, 6566.

(39) Xu, Y.; Ikeda, R.; Sugiyama, H. *J. Am. Chem. Soc.* **2003**, *125*, 13519.